Spring 5-31-2015

Characterizing alma for solar observation

Yi Chai
New Jersey Institute of Technology

Copyright Warning & Restrictions

The copyright law of the United States (Title 17, United States Code) governs the making of photocopies or other reproductions of copyrighted material.

Under certain conditions specified in the law, libraries and archives are authorized to furnish a photocopy or other reproduction. One of these specified conditions is that the photocopy or reproduction is not to be "used for any purpose other than private study, scholarship, or research." If a, user makes a request for, or later uses, a photocopy or reproduction for purposes in excess of "fair use" that user may be liable for copyright infringement,

This institution reserves the right to refuse to accept a copying order if, in its judgment, fulfillment of the order would involve violation of copyright law.

Please Note: The author retains the copyright while the New Jersey Institute of Technology reserves the right to distribute this thesis or dissertation

Printing note: If you do not wish to print this page, then select "Pages from: first page # to: last page #" on the print dialog screen

ABSTRACT

CHARACTERIZING ALMA FOR SOLAR OBSERVATION

by
Yi Chai

ALMA (Atacama Large Millimeter/submillimeter Array) is an antenna array of 66 antennas located in northern Chile at 5000 meters altitude. It is the largest ground-based array operated at millimeter/submillimeter wavelengths. In this thesis, the advantages of using ALMA for solar observation are presented, together with the introduction of a campaign to commission ALMA for solar observations. Observation modes of the solar campaign are reviewed in Chapter 2. Methods for constructing images from single dish data as well as the procedure for processing interferometer data, including calibration and imaging, are given in Chapter 3. The CLEAN algorithm that is used for producing images is also discussed in this chapter. Examples of processed images, both for single dish and interferometer, are shown in Chapter 4. In the final Chapter 5, a discussion about what remains to be done to create the observing tool and define observing modes for future ALMA solar campaign is provided.

CHARACTERIZING ALMA FOR SOLAR OBSERVATION

by
Yi Chai

A Thesis
Submitted to the Faculty of
New Jersey Institute of Technology
and Rutgers State University New Jersey-Newark
in Partial Fulfillment of the Requirements for the Degree of
Master of Science in Applied Physics

Department of Physics

May 2015

APPROVAL PAGE

CHARACTERIZING ALMA FOR SOLAR OBSERVATION

Yi Chai

Dr. Dale E. Gary, Thesis Advisor — Date
Distinguished Professor of Physics, NJIT

Dr. Haimin Wang, Committee Member — Date
Distinguished Professor of Physics, NJIT

Dr. Andrew J. Gerrard, Committee Member — Date
Professor of Physics, NJIT

BIOGRAPHICAL SKETCH

Author: Yi Chai

Degree: Master of Science

Date: May 2015

Undergraduate and Graduate Education:

- Master of Science in Applied Physics,
  New Jersey Institute of Technology, Newark, NJ, 2015
- Bachelor of Science in Astronomy,
  Peking University, Beijing, People's Republic of China, 2011

Major: Applied Physics

I don't pretend to understand the universe - it's much bigger than I am.

Albert Einstein

ACKNOWLEDGMENT

I would like to thank Professor Dale Gary for his excellent guidance of my thesis and the permission to let me join the ALMA solar campaign and use the observing data for my master thesis. I would like to thank everyone in the ALMA solar campaign group for sharing their knowledge. It gives me a great improvement in my ability of doing research in astronomy. I would also like to thank all the committee members for their corrections to my thesis, from which I learned a lot. Last but not least, I want to thank my family for supporting my study in America. Without their help I could not have made such progress in just two years.

TABLE OF CONTENTS

LIST OF TABLES

LIST OF FIGURES

CHAPTER 1

INTRODUCTION

1.1 Introduction of ALMA

The Atacama Large Millimeter/sub-millimeter Array (ALMA), an international partnership of the European Organization for Astronomical Research in the Southern Hemisphere (ESO), the U.S. National Science Foundation (NSF) and the National Institutes of Natural Sciences (NINS) of Japan in cooperation with the Republic of Chile, is the largest astronomical project in existence.

The start of the ALMA project dates back to the end of last century, when the North American community, represented by NSF and the European community, represented by ESO signed the first memorandum in 1999. An agreement was then reached in 2002 about the construction of ALMA on a plateau in Chile. Thereafter, the NAOJ (National Astronomical Observatory of Japan) joined the plan, and an official trilateral agreement between ESO, the NSF and NINS of Japan concerning the construction of the enhanced ALMA, was signed in September 2004. This agreement was later amended in July 2006 [1].

ALMA Early Science operations started with Cycle 0 in September 2011, two years before construction was complete. The current call for proposals, Cycle 3, is still within the Early Science period, in which case a reduced number of antennas, frequency bands, array configurations and observing modes will be available. The Solar commissioning study discussed in this thesis aims to provide the first call for solar observing proposals in Cycle 4 (Oct 2016).

1.1.1 The ALMA Telescope

ALMA is composed of 66 antennas, divided into two groups. The 12-m Array, consisting of 50 12-m antennas, is used for high-resolution imaging. The Atacama

Compact Array (ACA or Morita Array), consisting of 12 closely spaced 7-m antennas (the 7-m Array) and four 12-m antennas (the TP array, where TP stands for total power), is used for wide field imaging. Figure 1.1 shows ALMA in its most compact configuration.

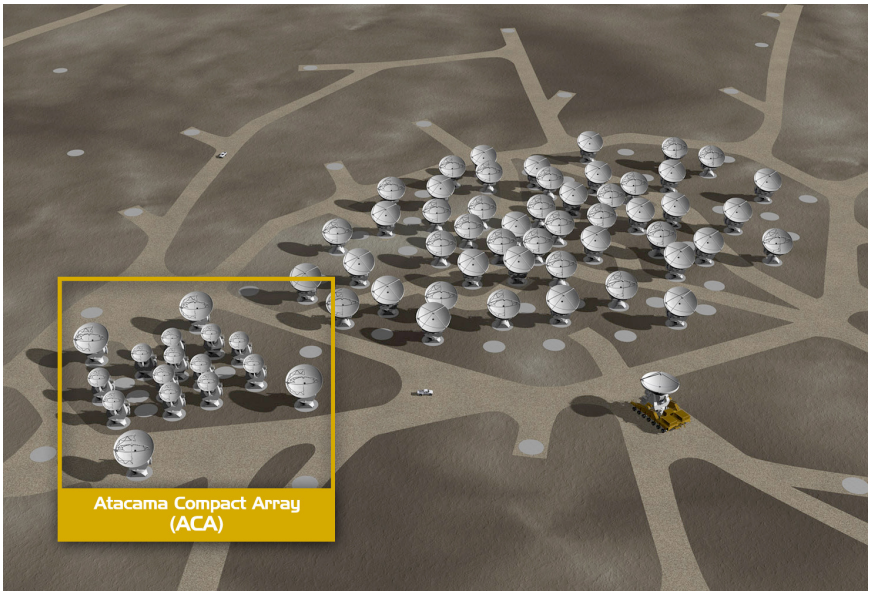

Figure 1.1 ALMA observatory in its compact configuration, with the ACA to the left. Some unoccupied stations can be seen, to which antennas of the 12-m Array can be moved by the transporter as the array is being reconfigured.

source: http://www.almaobservatory.org/en/visuals/images

The 12-m Array The 12-m Array consists of 50 12-m antennas designed and built by European and North American ALMA partners (each providing 25 antennas). Each antenna contains one front-end, including a cryostat, amplitude calibration device (ACD), water vapor radiometer (WVR), and backend electronics. There are four independent local oscillators (LOs) in the reference system so that the 7-m Array, the TP Array and two subarrays of the 12-m Array can make simultaneous, independent observations [2].

The Atacama Compact Array (The Morita Array) The ACA consists of 12 7-m antennas (the 7-m Array) for interferometry and four 12-m antennas (the TP Array) for single-dish observation. This array is designed to solve the "zero spacing" problem, which arises from the constraint that it is not possible to pack antennas closer than their diameter, and that problem will cause a hole in the distribution of the baselines at short and zero baseline separations. The four single-dish antennas provide spatial information samples equivalent to 0 m to 12 m, while the 7-m Array samples baselines from 9 m to 30 m [2]. The ACA is operated in a similar way to the 12-m Array. To achieve this unified operation, the ACA system is as compatible with the 12-m Array as possible at the level of hardware, interface, data collection, and observing modes. However, unlike the 12-m antennas, the 7-m antennas are not equipped with Water Vapor Radiometers (WVRs).

1.1.2 The ALMA Site

The array is located on the Chajnantor plain of the Chilean Andes (latitude = $-23.022917°$, longitude = $-67.754649°$), a site that normally offers the exceptionally dry and clear sky conditions required to observe at millimeter and submillimeter wavelengths. The ALMA site contains two main facilities. The ALMA antennas, weather stations, the two correlators and their computer interfaces, local oscillator generation hardware, timekeeping hardware, and the related array real-time machine computer are all located at the 5000 meters altitude site referred to as the Array Operations Site (AOS). This site is connected via gigabit fiber links to the Operation Support Facility (OSF), located at an altitude of 2900 m, about 22 km from the AOS and 40 km from the town of San Pedro de Atacama. Science operations are conducted from the OSF and coordinated from the Joint ALMA Observatory (JAO) Central office in Santiago [2].

A good observatory site must reach several standards. One important standard is the atmospheric window, which has to fit the telescope's wavelength coverage. The concept of an atmospheric window is formed from the fact that some wavelengths of electromagnetic radiation can pass through the atmosphere, while others do not. The ability of the atmosphere to allow radiation to pass through it is referred to as its transmission, and it varies with wavelength. The main reason for the variation is gas absorption. The gases that comprise our atmosphere, such as water vapor, carbon dioxide and ozone, absorb radiation in certain wavelengths, and the area in the spectrum absorbed by these gases are known as absorption bands. In contrast to the absorption bands, there exist areas of the spectrum where the atmosphere is transparent to certain wavelengths. Those wavelength bands are called atmospheric windows, since they allow the radiation to pass through the atmosphere. Figure 1.2 shows the transmission of the atmosphere for electromagnetic radiation over a range of frequency [3].

From Figure 1.2 we can see several absorption areas in the range of millimeter/submillimeter wavelengths. Among them, a very important contributor is water vapor absorption [4]. However, due to the extremely dry climate (PWV$\sim$1mm in August, as shown in Figure 1.3) and high altitude (5000 m) of Altiplano de Chajnantor plateau, ALMA is capable of detecting radio waves of millimeter and submillimeter wavelengths that would be completely absorbed at a lower, less dry site. Figure 1.3 shows the band 3 zenith transmission for 1, 5 and 15 mm of PWV, the atmospheric transmission can reach 0.95 for most of the bandwidth when PWV = 1 mm.

1.1.3 The ALMA Instruments

The ALMA front end can accommodate up to 10 receiver bands covering most of the wavelength range from 10 to 0.3 mm (30-950 GHz). Each receiver band is designed to

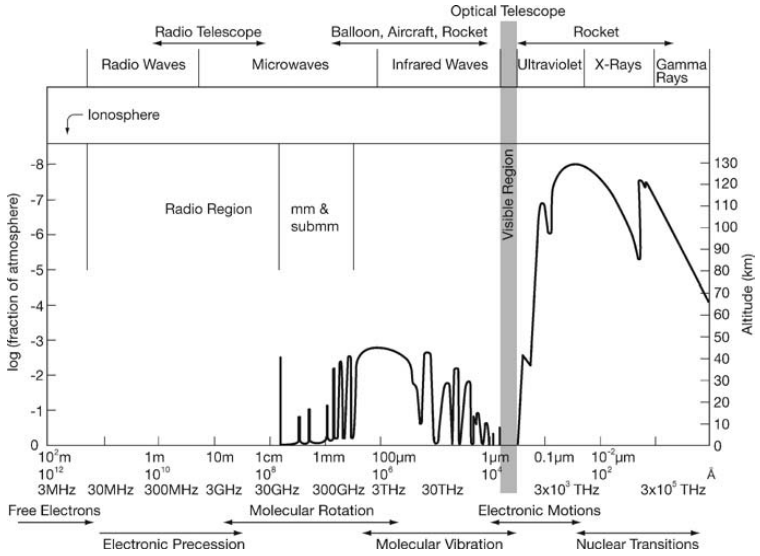

Figure 1.2 The transmission of earth's atmosphere for electromagnetic radiation. The diagram gives the height in the atmosphere at which the radiation is attenuated by a factor of 1/2.

source: Tools of Radio Astronomy, page 3 [3]

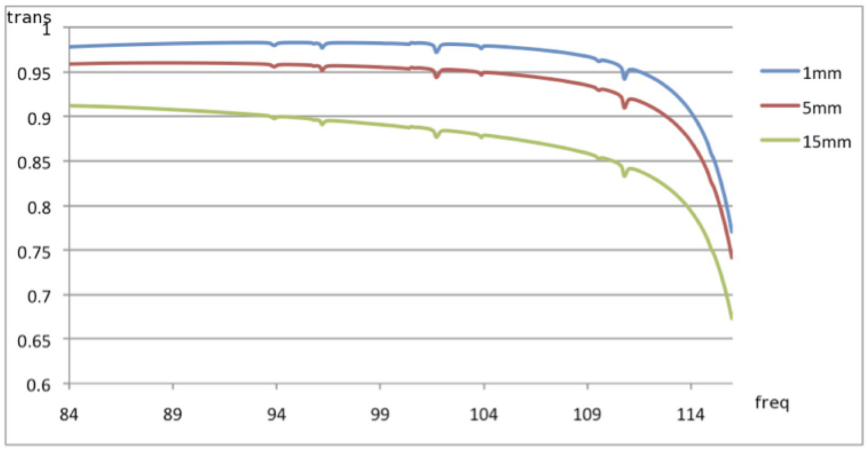

Figure 1.3 Band 3 zenith transmission for 1, 5, and 15 mm of PWV. Frequency is in GHz.

source: ALMA Cycle 3 Technical Handbook, page 36 [2]

cover a tuning range that is approximately tailored to the atmospheric transmission windows. The receivers are described in more detail in Table 1.1 and Figure 1.4

The observed sky frequencies need to be downconverted to frequency bands between 0-2 GHz in order to send the signals to the correlator. The frequency downconversion involves a set of local oscillators. The frontend mixer uses LO1 to downconvert the sky frequencies into an IF band with a range of 4-12 GHz. This covers the needs of all ALMA bands. For Band 3, 4, 7 and 8, the mixers have an output of 4-8 GHz, for Band 6 the range is 6-10 GHz and Band 9 and 10 the range is 4-12 GHz. The possible sky frequency ranges covered by each receiver with the first local oscillator set to a frequency F_{LO1} are:

For the lower sideband (LSB): $(F_{LO1} - IF_{lo})$ to $(F_{LO1} - IF_{hi})$

For the upper sideband (USB): $(F_{LO1} + IF_{lo})$ to $(F_{LO1} + IF_{hi})$

Table 1.1 Receiver Characteristics of ALMA[a]

Band	Frequency/ Wavelength range (GHz)[b]/(mm)	LO range (GHz)	Sideband mode[c]	IF range (GHz)	Inst. IF bandw. (GHz)[d]	T_{rx} over 80% of band (K)[e]	T_{rx} at any frq. (K)
3	84.0-116.0/ 2.59-3.57	92-108	2SB	4-8	7.5	<41	<45
4	125.0-163.0/ 1.84-2.40	133-155	2SB	4-8	7.5	<51	<82
6	211.0-275.0/ 1.09-1.42	221-265	2SB	5-10	7.5	<83	<136
7	275.0-373.0/ 0.80-1.09	283-365	2SB	4-8	7.5	<147	<219
8	385.0-500.0/ 0.60-0.78	393-492	2SB	4-8	7.5	<196	<292
9	602.0-720.0/ 0.42-0.50	610-712	DSB	4-12	7.5(15)	<175 (DSB)	<261 (DSB)
10	787.0.0-950.0/ 0.32-0.38	795-942	DSB	4-12	7.5(15)	<230 (DSB)	<344 (DSB)

[a]source: ALMA Cycle 3 Technical Handbook, page 32

[b]Frequency range is the maximum available, at the extreme upper and lower limits of the IF bandpass

[c]Sideband modes: SSB means single sideband receiver, 2SB means dual sideband receiver where the two sidebands are available simultaneously, DSB means double sideband receiver.

[d]Maximum instantaneous IF bandwidth: As both upper and lower sidebands both pass through the same IF bandwidth but are subsequently separated, the effective signal bandwidth given in this column for 2SB receivers is twice the actual IF filter bandwidth. In addition, this is per polarization, so the total effective bandwidth for each receiver is then another factor of 2 higher.

[e]List of the minimum specification of the SSB receiver temperature (T_{rx}), unless otherwise noted, is shown. These values are the average over the IF band.

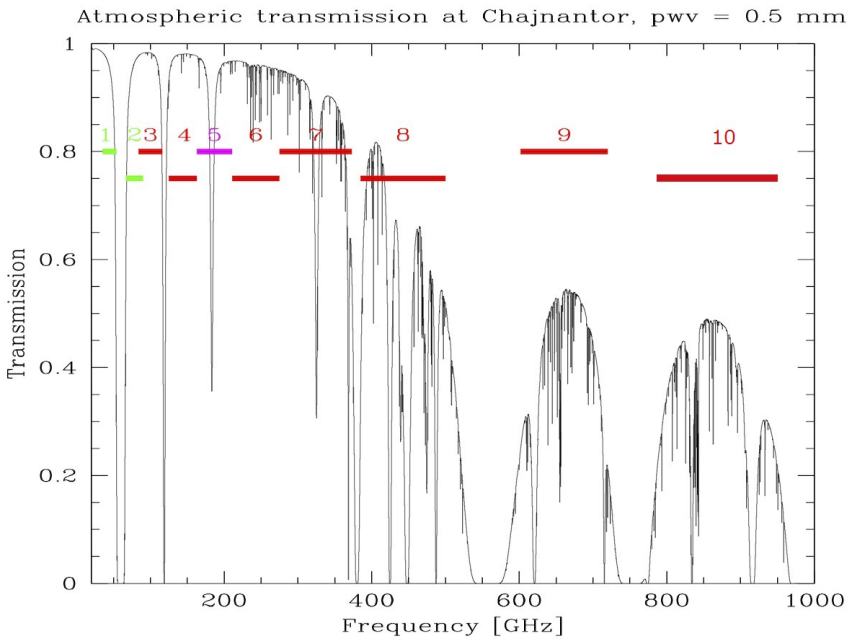

Figure 1.4 The ten ALMA receiver bands. The red line indicate the bands that can be used in Cycle 3.

source: ALMA Cycle 3 Technical Handbook, page 31 [2]

where IF_{lo} and IF_{hi} are the lower and upper IF ranges in the "IF Range" column of Table 1.1.

1.1.4 The Angular Resolutions of ALMA's Antennas

The angular resolution of a single-dish radio telescope can be described using equation:

$$\theta = \frac{k\lambda}{D} \tag{1.1}$$

where θ is the angular resolution, λ is the wavelength of the radiation received, D is the diameter of the instrument and k is a factor that depends on aperture geometry. For a single-dish telescope, the k factor is 1.22 [2]. According to Equation 1.1, the angular resolutions of ALMA's antennas, both 7-m and 12-m, are based on the receiver's frequency band. The calculation results of angular resolutions for different bands and

antennas are shown in Table 1.2. For each band, only the center frequency is used for the calculation.

Table 1.2 Angular Resolutions of ALMA's Antennas[a]

Band	Center Frequency (GHz)	Angular Resolution of 7-m Antenna (arcsecond)	Angular Resolution of 12-m Antenna (arcsecond)
3	100	107.8	62.9
4	144	76.2	44.5
6	243	45.1	26.3
7	324	34.0	19.8
8	442	24.8	14.5
9	661	16.5	9.6
10	868	12.6	7.3

[a]All angular resolutions are calculated using center frequency of each receiver bands

1.2 ALMA Solar Commissioning

ALMA opens a new window for solar physics studies. With the high-precision antennas operated in the wavelengths of millimeter and submillimeter, we can study the heating and dynamics of the sun's chromosphere. Other science goals including studies of the origin of fast solar wind, solar filaments, coronal cavities, precursors to coronal mass ejections, sunspots and active regions, can also be achieved. ALMA will serve as an important asset that complements the Very Large Array (VLA) and the Expanded Owens Valley Solar Array (EOVSA), Big Bear Solar Observatory (BBSO), Solar Dynamics Observatory (SDO) and others planned for the future.

The millimeter/submillimeter radiation of the quiet Sun originates from the base of the chromosphere up to the middle chromosphere. The source can be described using the Planck function [5]:

$$B(\nu, T) = \frac{2h\nu^3}{c^2} \frac{1}{e^{\frac{h\nu}{k_B T}} - 1} \tag{1.2}$$

Moreover, consider the Rayleigh-Jeans approximation, since the wavelength (∼1 mm) and temperature (∼6000 K) gives $\frac{h\nu}{k_B T} \sim 2.4 \times 10^{-3}$, we can expect a good approximation to Rayleigh-Jeans law. According to the Rayleigh-Jeans law, we have:

$$B(\nu, T) = \frac{2\nu^2 k_B T}{c^2} \tag{1.3}$$

The observed flux density at millimeter/submillimeter is therefore linearly related to the temperature of the emitting plasma, which makes it capable of serving as a linear "thermometer" to probe the lower solar atmosphere.

1.2.1 ALMA Solar Observing Campaign

The ALMA Solar Observing Campaign (ASOC) is performed by an international group consisting of scientists from both North America and Europe. The goals of the ASOC include developing observing strategies to address solar science objectives, developing and testing data calibration and imaging procedures, and defining requirements for supporting software.

1.2.2 Science Objectives of ASOC

Due to the advantages of ALMA, a number of science objectives can be studied. Some key science objectives are listed below [5]:

The Quiet Sun Chromosphere: The early studies of the quiet Sun demonstrated that the chromosphere is far from hydrostatic equilibrium. It is in constant motion as a result of turbulent motions of the underlying photospheric convection, and the fractional ionization varies by orders of magnitude from the temperature minimum

region to the base of the corona, as does the plasma beta in the magnetized chromosphere. Chromospheric heating and dynamics are considered to be one of the biggest challenges in solar physics, and we can expect ALMA to make advances in this area, since millimeter observation has natural advantages for observing the lower solar atmosphere, such as its linear dependence on temperature, compared with other observations in different wavelength regions.

Active Regions and Sunspots: Active regions are associated with flares and coronal mass ejections. They correspond to magnetic fields that have erupted through the sub-photospheric surface up into the corona. Sunspots are considered to have the strongest magnetic fields. Due to their physical characteristics, multi-band measurements of the active regions and sunspots will be of key interest. Together with polarization measurements, they can be used to construct the structure of the solar atmosphere in both strong and weak magnetic environments.

Prominences and Filaments: Solar filaments are characterized by cool, filamentary material suspended in the solar corona above magnetic neutral lines. They typically appear dark when seen in absorption against the solar disk at wavelengths longer than a few mm. They are seen in emission as prominences above the limb. They can erupt in association with a coronal mass ejection. Their formation, stability and eventual eruption are therefore key research topics. High resolution observations by ALMA will enable new constraints to be placed on their structure (temperature, density, magnetic field) and the evolution thereof as they approach instability.

Solar Flares: Flare emission involves several emission mechanisms. Synchrotron emission yields insights to the acceleration and transport of the most energetic electrons accelerated in flares, those with energies in the MeV to 10s of MeV range. Unlike gyrosynchrotron radiation from flares at centimeter wavelengths and longer,

where the Faraday depth of the corona is very large, it may be possible to detect and exploit linearly polarized radiation from the synchrotron emission from flares at millimeter/submillimeter wavelengths.

1.2.3 The Author's Role in ASOC

The ALMA Solar Observing Campaign is a large collaboration, with essential contributions from many individuals. The U.S. part of the project is led by Dr. Timothy Bastian, but includes 13 other members from the U.S. and elsewhere. The project also is linked with a parallel team of 23 scientists sponsored by ESO.

The observations obtained for characterizing ALMA for solar science were shared among all team members, who individually produced images and compared them, as well as evaluating different modes of taking the data. The author led the effort to calibrate the data at NJIT under the directions of Professor Gary, and produced the single-dish and interferometric images for comparison with works of other team members. The author investigated strategies for analyzing and displaying the single-dish fast scanning images. The author also took the analysis scripts created by Dr. Masumi Shimojo and adapted it for different observing modes to produce many of the figures shown later in this thesis.

CHAPTER 2

OBSERVATIONS

The ALMA Solar Observing Campaign can be separated into single-dish observation and interferometric observation. Both observations are challenging because of the high radiance of the Sun. The quiet Sun radiates of 5000-6500 K within the ALMA frequency range, while flares can generate 3000-30000 K additional antenna temperature, or even more for big flares [6]. This is too high for standard calibration since the calibrator sources such as quasars and planets have a much weaker signal.

In order to reduce the flux intercepted by ALMA, an attenuator device called the solar filter, has been designed and installed on the Amplitude Calibration Device. The attenuation level is frequency dependent, with higher attenuation at low frequency and lower attenuation at high frequency. However, one can not use the solar filter on calibrators, so a new flux calibration method has to be developed for solar observations without the solar filter.

Another way to increase the upper level of ALMA receivers' dynamic range is to de-tune the SIS mixers to increase their saturation level [6]. The de-tuning modes used in ALMA Solar Observing Campaign are shown in Table 2.1

Table 2.1 Parameters of Solar Mode[a]

Mode Name	Band	Mixer Tuning	IFswitch ATT	IFproc ATT	ifLevel (Optimization)
Band3-solar1	3	solar1	-8 dB	-10 dB	-20 dBm
Band3-solar2	3	solar2	-8 dB	0 dB	normal
Band6-solar1	6	solar1	-5 dB	-10 dB	-20 dBm
Band6-solar2	6	solar2	-8 dB	0 dB	normal

[a]The mixer tuning of solar1 with Band6 is the same as the normal setting [7]

2.1 Single Dish Observation

The single dish observations are designed to develop a flux calibration scheme in order to solve the problem we just mentioned. From the interim report of single dish flux calibration (Masumi Shimojo, JIRA: CSV-2925) [8], a equation is derived based on the following assumptions: 1. The Earth's atmosphere in the direction of the Sun is same as that towards the calibrator (a planet). 2. The elevation angle of the Sun is the same as the planet. 3. The solar filter works as just an attenuator. Which will lead to:

$$T^*_{sun} = \frac{P_{sun} - P_{sky}}{P_{planet} - P_{sky}} T^*_{planet} \tag{2.1}$$

where P_{sky}, P_{sun} and P_{planet} are the output auto-correlation values from the correlator, and T^*_{sun} and T^*_{planet} are the brightness temperatures of the Sun and planet, respectively. By using this equation, we can calculate the antenna temperature of the Sun based on the observing value of the sky, planet and Sun.

Single dish observations can be done in several observing modes. The mode is important in the case of solar flare observations, since we cannot predict when and where a flare will occur. A general solution is to use fast mapping strategies that make use of the high performance tracking capabilities of ALMA. Such modes can potentially map limited areas (in the case of solar flares, they can be active regions) of the Sun in seconds, or the full scan in 5 minutes.

Some of the scan patterns explored in the ASOC are shown in Figure 2.1 and Figure 2.2. The idea is presented by Richard Hills in a memo [9].

As shown in Figure 2.1, for the Lissajous scan pattern, each antenna axis is driven by a sine wave. The Lissajous curve can be described using parametric equations:

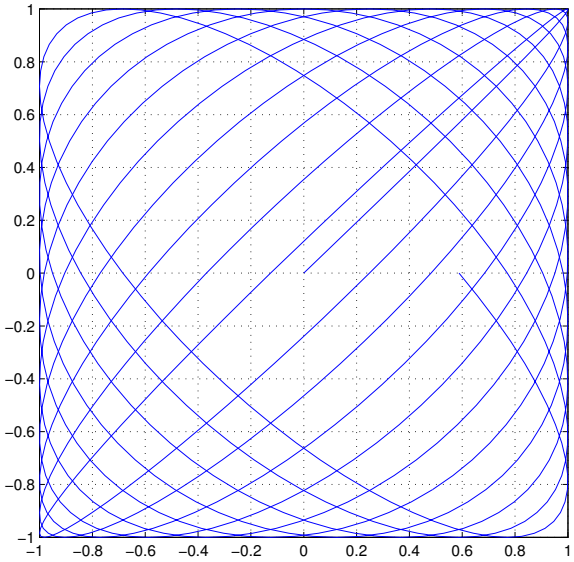

Figure 2.1 An example of Lissajous scan pattern. Generated using Matlab, with A and B set to 1, $n = 1.04$, δ=0 (see Equation 2.2).

$$\begin{cases} X = A\sin(nt + \delta), \\ Y = B\sin(t) \end{cases} \tag{2.2}$$

where $0 \leq \delta \leq \frac{\pi}{2}, n \geq 1$. This kind of curve is used in describing the two-dimensional harmonic oscillator, in which case the phase difference can be arbitrary. The Lissajous curve was first investigated by Nathaniel Bowditch in 1815, and later in more detail by Jules Antoine Lissajous in 1857 [10]. When used in guiding the telescope, the phase difference, δ, is usually set to 0 so that the scan pattern can pass through the center of the field, and in order to generate a compact curve, the frequency difference $(n-1)$ is set to a small value.

The Double Circle pattern is simpler. Each antenna axis is driven by the sum of fast and slow sine waves with the same frequencies and 90°phase difference. Therefore the parametric equations of the Double Circle curve can be written as:

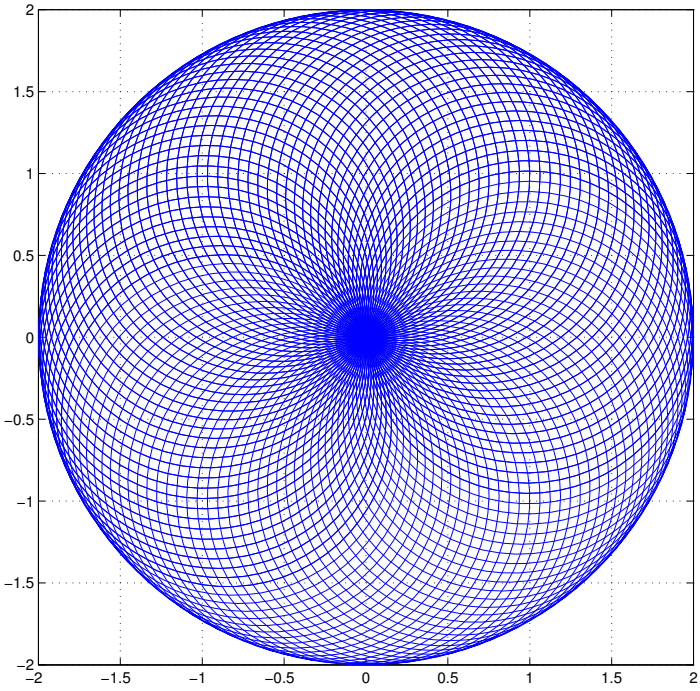

Figure 2.2 An example of Double Circle scan pattern. Generated using Matlab, with A and A′ set to 1, $n = 100$ (see Equation 2.3).

$$\begin{cases} X = A\cos(t) + A'\cos(nt), \\ Y = A\sin(t) + A'\sin(nt) \end{cases} \tag{2.3}$$

where $A' = A$. When used in guiding the telescope, the A' is often set to be smaller than A, by doing that, it will generate a hole in the center of the scan pattern so the overshoot effect causing by movement of the dishes is compensated [9].

2.2 Interferometric Observation

The limitation of single-dish radio antennas can be illustrated using Equation 1.1. For a given wavelength, to improve angular resolution, the diameter D must be increased. However, limited by material and technology, the diameter of the biggest single-dish radio telescope is still in the scale of hundreds of meters (already existing: The Arecibo Observatory, 300m [11]. Under construction: the Five-hundred-meter Aperture Spherical Telescope, 500m [12]). This limitation is no longer important when using interferometers. In this case, D becomes the largest spacing between two antennas in the array, or the longest baseline. By modifying the array, we can have a baseline even comparable with the diameter of earth ($\sim$8000 km baseline, Very Long Baseline Array [13]). For ALMA , the longest baseline can reach 16 km [2] for the 12-m Array, which corresponding to the spatial angular resolution of 5 milliarcseconds at 950 GHz.

At the time of the December 2014 ALMA Solar Observing Campaign, the array configuration was as shown in Figure 2.3. The longest baseline of this relatively compact configuration was $\sim$350 m, which gives the angular resolution shown in Table 2.2. Angular resolutions of other array configurations with the longest baseline equals to 16 km (maximum baseline length) and 160 m (minimum baseline length) are also shown in Table 2.2

Table 2.2 Angular Resolutions of Synthesized Beam[a]

Band	Angular Resolution of conf.1(350m) (arcsec)	Angular Resolution of conf.2 (3km) (arcsec)	Angular Resolution of conf.3 (16km) (arcsec)
3	**1.7**	**0.21**	0.039
4	**1.2**	**0.15**	0.027
6	**0.74**	**0.086**	0.016
7	**0.56**	**0.065**	0.012
8	**0.41**	0.047	0.0089
9	**0.27**	0.032	0.0059
10	**0.21**	0.024	0.0045

[a]All angular resolutions are calculated using center frequency of each receiver bands, The data are retrieved from Table 1.2

For the Sun, angular resolution below ∼0.05 arcsec is not expected, and therefore arrays larger than a certain, band-dependent level are not suitable for solar observations. Acceptable frequency band and array configuration are shown in bold face.

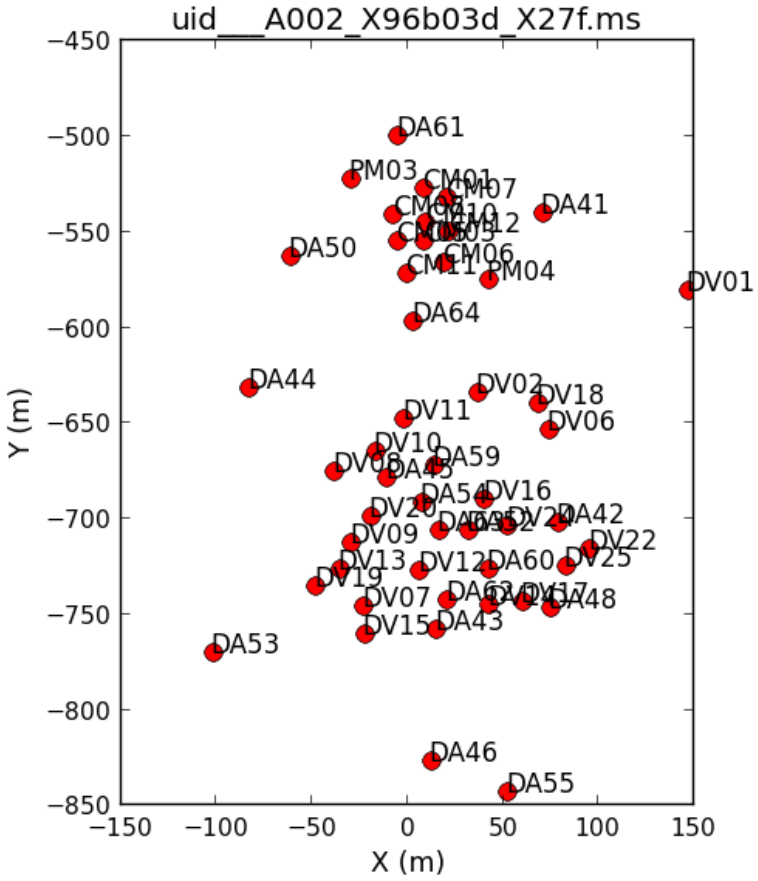

Figure 2.3 Array configuration. Generated using CASA. The antenna name indicates the array type and manufacturer of the antennas. In this case, DV stands for ALMA 12-m (Vertex) antennas, DA stands for ALMA 12-m (AEM) antennas, CM stands for ALMA ACA 7-m antennas and PM stands for ALMA ACA 12-m TP antennas [14].

CHAPTER 3

TECHNIQUES

3.1 Single Dish Data Processing

According to the scan pattern, we know that not all parts of the Sun are sampled, while the rapid movement of the pointing position of antenna may also cause differences between the actual scan pattern and the ideal scan pattern [9]. However, if we slow down the scanning and/or use a dense sampling to get a more accurate scan pattern, the fluctuations in the emission from the atmosphere and in the gain of the receivers will increasingly affect the stability and reliability of the measment. In that case, the problem is far more complicated.

In order to fill in the unsampled areas missed by the scan pattern, we have to interpolate reasonable values from the original data. The processing can be done by using Matlab. In Matlab, the original image is treated like a surface which is described as: $v = f(x, y)$ where $f(x, y)$ fits the scatted data in vectors (x, y, v). A grid is generated by the "meshgrid" function in Matlab to give the points that later on can be used for interpolation. The "griddata" function then uses these points as new coordinate values to interpolate the surface $v = f(x', y')$ where (x', y') are coordinates on a regular grid, and returns the corrected image. The equivalent processing can be done with IDL's "triangulate" and "trigrid" functions. The Matlab script is shown in Appendix A.

The full disk solar images taken in September, 2014 are shown in both Figure 3.1 and Figure 3.2. The Lissajous scan pattern is used in Figure 3.1 and Double Circle scan pattern is used Figure 3.2. The left-side images of both figures are generated using Matlab command "scatter" to demonstrate the unsampled areas causing by the scan pattern, while the right-side images of both figures show the interpolated results as a comparison. For both figures, the data were taken in December 2014

(JIRA: CSV-3166) [15]. The Double Circle pattern has a more uniform sampling, and the added advantages that each cycle samples the same point in the center of the field. By normalizing each sweep to the same value at this point, fluctuation in the atmospheric absorption can be minimized (under the assumption that the solar variations are neglectable).

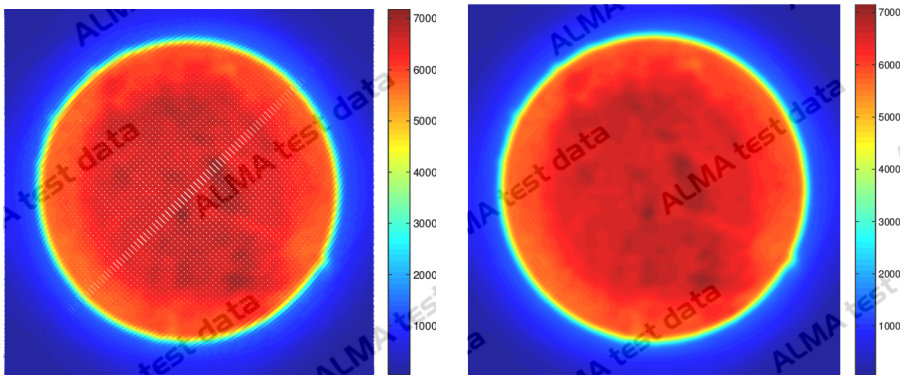

Figure 3.1 Image of the whole Sun with Lissajous scan pattern. Data were taken using band 3 receiver. The left-side figure is generated using Matlab command "scatter" while the right-side figure shows the interpolated image.

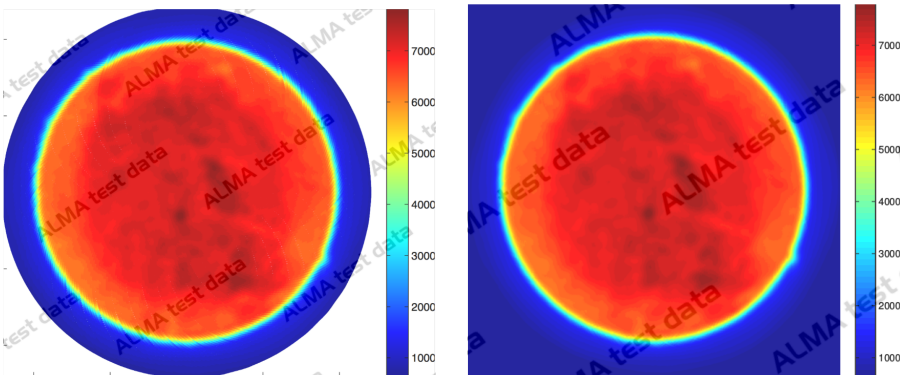

Figure 3.2 Image of the whole Sun with Double Circle scan pattern. Data were taken using band 3 receiver. The left-side figure is generated using Matlab command "scatter" while the right-side figure shows the interpolated image.

According to the raw data, the total number of data samples and time separation between each point is fixed and the same for both scan patterns. So we can easily calculate the "effective" data ratio for both Lissajous and Double Circle scan patterns

by setting a threshold for the data. A datum is called "effective" when it contains the solar data as opposed the blank sky. In the case of solar observations, since the data represent the temperature of chromosphere, the threshold can be set equal to 6000 for the full-Sun observation. For the Double Circle scan pattern, the effective data ratio is 0.5793, and for Lissajous scan pattern the ratio is only 0.1642, due to the amount of time the Lissajous sweep spends near the edges (off-Sun) of the scan (see Figure 2.1).

When the observation field comes to a restricted area of the Sun, the concept of "effective" data is not fitting anymore, since the whole field may be on the solar disc and exceed the threshold temperature (e.g., an active region scan). In that case, other considerations are needed to judge which scan pattern is best for the situation. Figure 3.3 gives the interpolated image of a restricted area scan on active region AR12237. Here, band 3 (3 mm) is used for the observation.

A further image reduction can be done in order to eliminate the fluctuations mentioned before. For the Lissajous scan pattern, according to the Equation 2.2, we can expect a fixed number of data points for every circle of scan. When processing the data from an active region, a reasonable assumption can be proposed that adjacent curves have very similar total power due to small size of the field. In order to amend the data, the total power ratios of every adjacent curve can be calculated and used for correction.

3.2 Interferometer Data Processing

The complete procedure for interferometer data includes two steps, the first one is data calibration, and the second one is imaging. In this section, the data taken during December 12, 2014 from 19:25 UT - 20:12 UT are used to illustrate the whole procedure. The ALMA observation id is: uid://A002/X96b03d/X27f [7]. Within this time period, an observation was done on active region NOAA12237, using receiver

Figure 3.3 Interpolated image for AR12237 at 3 mm wavelength (band 3). Ten scans were done over 10 minutes with 1 image per minute. This figure only shows the first image [15]. Also the scan pattern is Lissajous scan pattern

band 6 (1 mm). CASA (the Common Astronomy Software Application), is software developed by the scientists from the National Radio Astronomical Observatory (NRAO), the European Southern Observatory (ESO), the National Astronomical Observatory of Japan (NAOJ), the CSIRO Australia Telescope National Facility (CSIRO/ATNF), and the Netherlands Institute for Radio Astronomy (ASTRON) [16].

3.2.1 Calibration

A typical data calibration routine includes: T_{sys} and WVR calibration table generation, flagging the bad data, T_{sys} and WVR calibration by applying the calibration tables, Bandpass calibration table generation, Gain Calibration table generation and applying both of these calibration tables to the data.

T_{sys} and WVR calibration The first phase of calibration includes two important steps: the System Temperature (T_{sys}) and Water Vapor Radiometer (WVR) calibration. However, in the ALMA Solar Observing Campaign, the interferometer includes both 12-m antennas and 7-m antennas. Since the WVR calibration cannot be done to the 7-m antennas, the WVR calibration part is neglected. The solar observation summary shows that only spectral windows number 1, 3, 5 and 7 contain useful data, so only these spectral windows are used to generate the T_{sys} calibration table.

Flagging After generating the calibration table of system temperature, we plot the system temperature for every antenna in the array to check which antenna has bad system temperature compared with others so that we can "flag" out the data generated by those antennas. Figure 3.4 shows the T_{sys} of all the antennas in the first solar scan as a function of frequency channels. From the figure we know that by taking out antenna DA61, DV01 and DV11 from the data set we can reduce the

system temperature, thereby increasing the signal-to-noise ratio. Since only spectral windows number 1, 3, 5 and 7 contain the usable data, those data are split into separate data files for further processing.

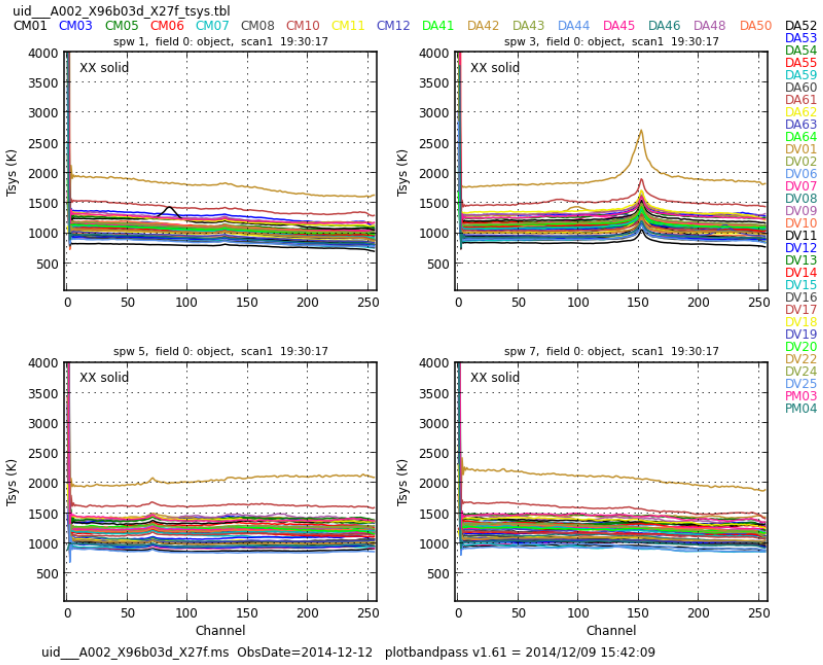

Figure 3.4 T_{sys} of all the antennas. Generated using CASA from solar observation, uid://A002/X96b03d/X27f. The figure shows the plots from spw 1, 3, 5 and 7. A set of antennas is "flagged" out due to abnormal system temperature compared with others, which means difference in the shape of curve or extremely high T_{sys} compared with the average system temperature. Antennas are marked with different color to in help the flagging procedure.

Bandpass calibration and Gain calibration Bandpass and Gain calibration are important because these two steps correct the phase and flux density of the data. In general, we can write a function that describes the relation between observed visibilities (V_{obs}) and true visibilities (V):

$$V_{ij}(t,\nu)_{obs} = V_{ij}(t,\nu)G_{ij}(t)B_{ij}(t,\nu) \tag{3.1}$$

where t is time, ν is frequency, i and j refer to a pair of antennas (i, j). G is the complex "continuum" gain, and B is the complex frequency-dependent gain (the "bandpass"). The Bandpass calibration is the procedure that corrects the frequency-dependent part of the gains, B_{ij}, while Gain calibration focuses on the time-dependent part. After finishing the flagging, a phase-only calibration table is first generated and applied to get the Bandpass calibration table. Then the Bandpass calibration table is used for getting the Gain calibration table. Both Bandpass and Gain calibration tables are applied to the original data file to get the corrected data. Figure 3.5 shows the Gain calibration table for 4 selected antennas in gain amplitude vs. time. After all the corrections are applied, the corrected data of both Sun and calibrators are split in order to generate the corrected databases, which is needed in the final image processing.

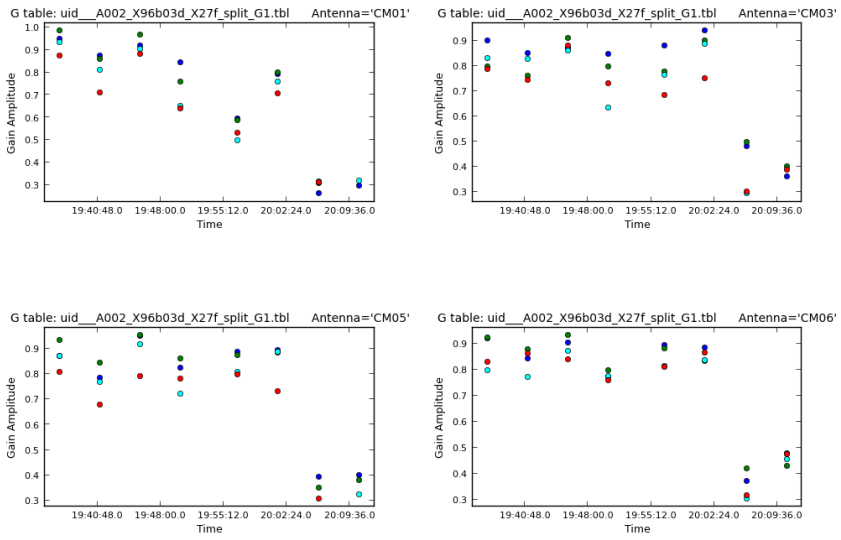

Figure 3.5 Gain calibration table in gain amplitude vs. time for 4 selected antennas. Different colors indicate different spectral windows. Generated using CASA from solar observation, uid://A002/X96b03d/X27f. Only shows the first 4 antenna's images

3.2.2 Imaging

After all the calibration is done, the "CLEAN" algorithm is used to generate the clean image.

CLEAN algorithm The intensity distribution $I_0(l, m)$ obtained in synthesis mapping can be written as a function of true intensity $I(l, m)$ convolved with the synthesized beam $b_0(l, m)$ [17]:

$$I_0(l, m) = I(l, m) * b_0(l, m) \tag{3.2}$$

Mathematically, $I(l, m)$ can be solved if we know $I_0(l, m)$ and $b_0(l, m)$. An analytic procedure for deconvolving two functions is to take the Fourier transform of the convolution, which is equal to the product of the Fourier transforms of the components. However, since there exist unsampled areas of the (u, v) plane, we can add an arbitrary visibility value to the unsampled areas, and the Fourier transform of these added values constitutes an invisible distribution that can not be detected, therefore we can have an infinite number of solutions to the convolution equation [18].

One of the most successful deconvolution procedures is the CLEAN algorithm devised by Högbom (1974) [19]. This is basically a numerical deconvolving process applied in the spatial (l, m) domain. It can be done by following these steps: 1. Compute the "dirty map" and the "dirty beam", which are the terms used for the synthesized intensity and the synthesized beam image. 2. Find the highest intensity point on the map and subtract the response to a point source, including the full sidelobe pattern, centered on that position. The peak amplitude of the subtracted point source is equal to γ times the corresponding map amplitude, where γ is called the loop gain, typically 0.1 or 0.05. Record the position and amplitude of the component removed by inserting a δ-function component into a model that will become the cleaned map. 3. Repeat procedure 2 until a certain threshold is reached. The

remaining flux is called residuals. 4. Replace all δ-functions in the cleaned model by a clean-beam of corresponding amplitude. The clean-beam is often chosen to be a Gaussian function with half-amplitude width equal to that of the dirty beam. 5. Add the residuals into the clean-beam map.

It is assumed that each dirty-beam response subtracted represents the response to a point source. Högbom(1974) has pointed out that much of the sky is a random distribution of point sources on an empty background, and CLEAN was initially developed based on that idea. By this assumption, the arbitrary value problem is eliminated, because the value of the non-sampled area is not arbitrary at all. A point source in the (l, m) plane will generate a complex sinusoid that extends in the (u, v) plane, no matter whether measured or not.

After applying the CLEAN algorithm to get the image, the data processing is finished for the raw data of ALMA. The CASA script used for calibration and imaging is originally provided by ASOC team members Bin Chen and Masumi Shimojo, although some specific modification is made in order to fit our case. The complete calibration and imaging script is attached in Appendix B.

CHAPTER 4

RESULTS

4.1 Single Dish Imaging

Figure 4.1 shows a comparison of images between ALMA (single dish with receiver band 6, ∼230 GHz) and Kanzelhöhe Observatory (H_α). The Kanzelhöhe's image has a better resolution due to the observing wavelength (H_α), which is ∼6563 angstroms. The angular resolution of Kanzelhöhe can reach ∼1 arcsecond. Although not having such a high-resolution result, the ALMA single-dish observation still provides enough information for seeking solar flares, which is one of the uses of the single-dish observation. Figure 4.2 shows another image taken on September 20 2014, which illustrates the details in partial disk scans done in several regions of the Sun.

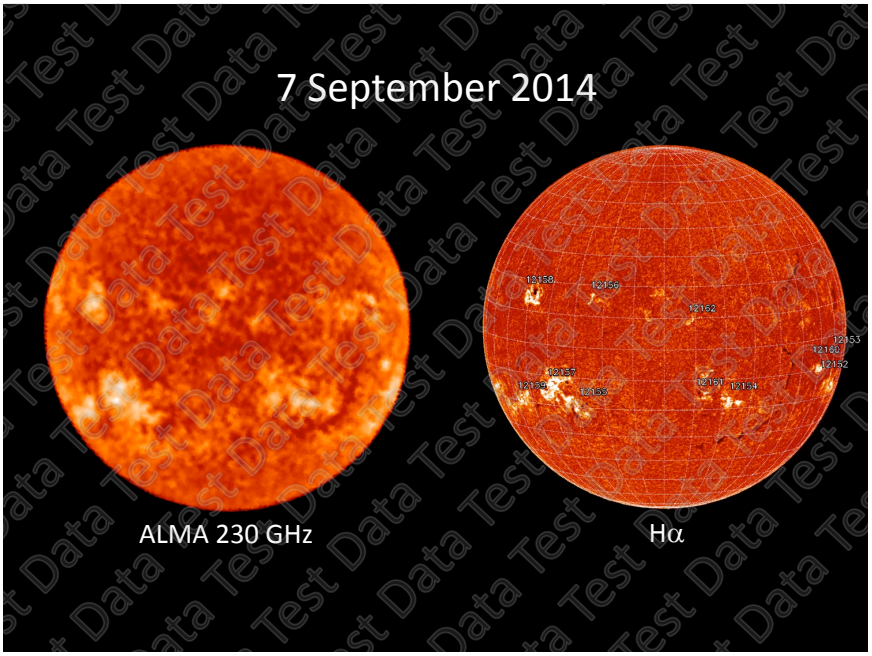

Figure 4.1 A comparison between the ALMA single-dish image and Kanzelhöhe Observatory H_α image. The data used to generate the ALMA image was taken on September 7 2014. The images are provided by ASOC team member Timothy Bastian.

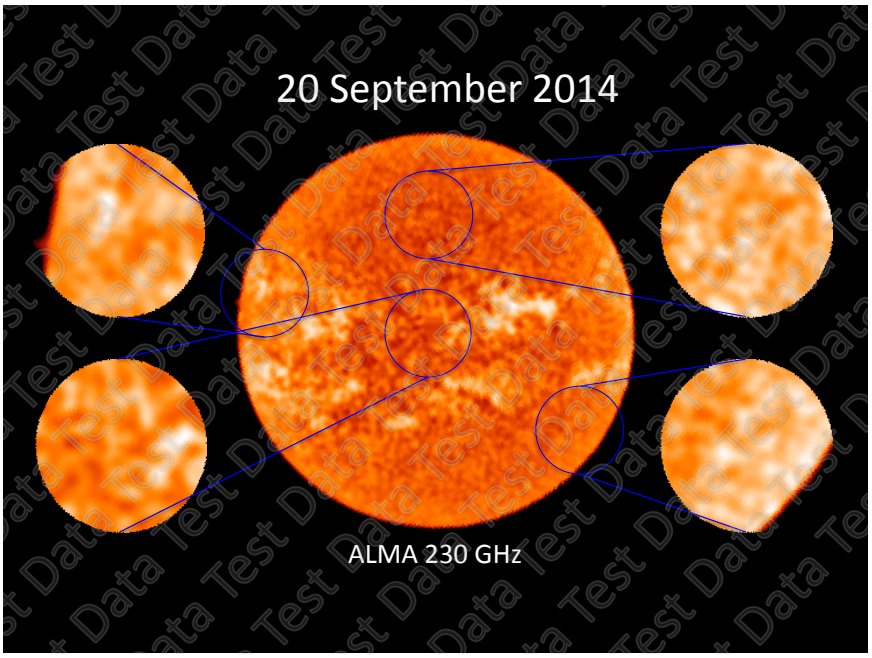

Figure 4.2 Partial images in relation to the full-disk image. The data used to generated this image were taken on September 20 2014. The image is provided by ASOC team member Timothy Bastian.

4.2 Interferometric Imaging

Figure 4.3, Figure 4.4 and Figure 4.5 show the images of several positions in active region NOAA12230. For Figure 4.3, the data were taken using band 6, and the SIS tuning mode is solar1, For figure 4.4, the corresponding mode is band6-solar2 and for Figure 4.5 it is band3-solar2 [7].

Comparing between band 6 and band 3, we can easily see that band 3 has a larger field of view while band 6 has a smaller field of view but 3 times higher the resolution. However, it is hard to compare SIS tuning mode solar 1 and solar 2 only using Figures 4.3 and 4.4, because they point to different positions within active region NOAA12230. A possible solution is to overlay the two images on a 3rd image (test image), which has a field wide enough for both images, and comparing the structures between them. A decision about which tuning mode is better can be made according to how well the corresponding image fits the test image.

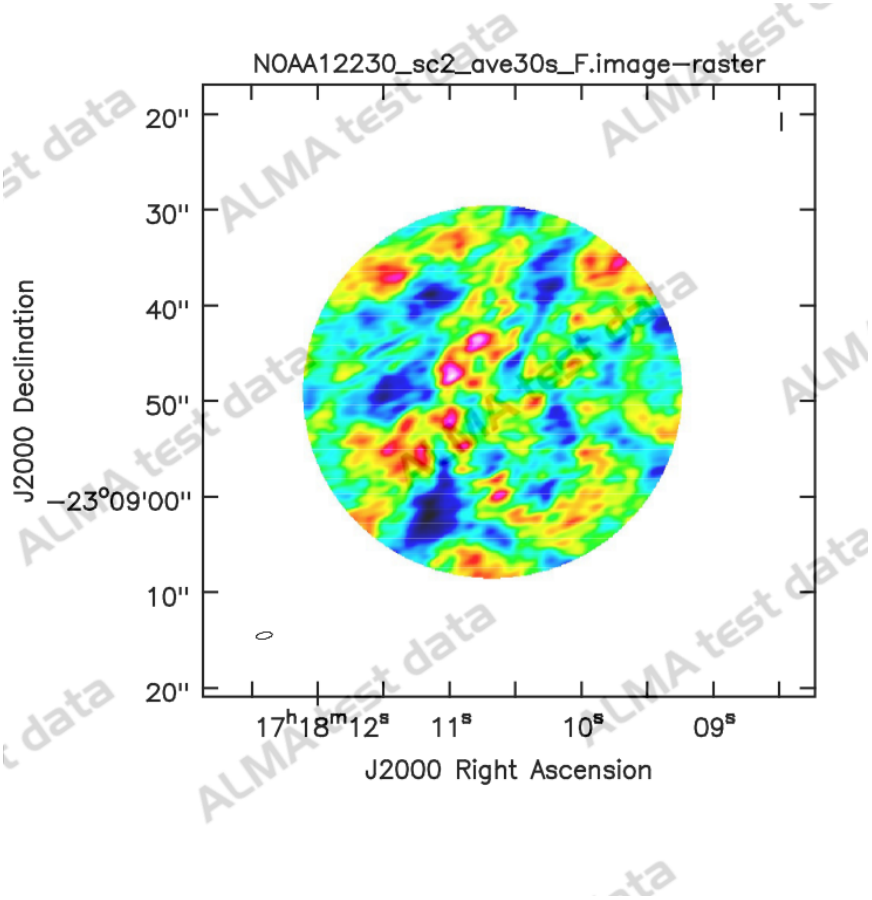

Figure 4.3 image of NOAA12230 after CLEAN. Generated using CASA from solar observation uid://A002/X96b03d/X226, which took part in December 12 2014 from 18:37 UT to 19:25 UT. The corresponding de-tuning mode is band6-solar1.

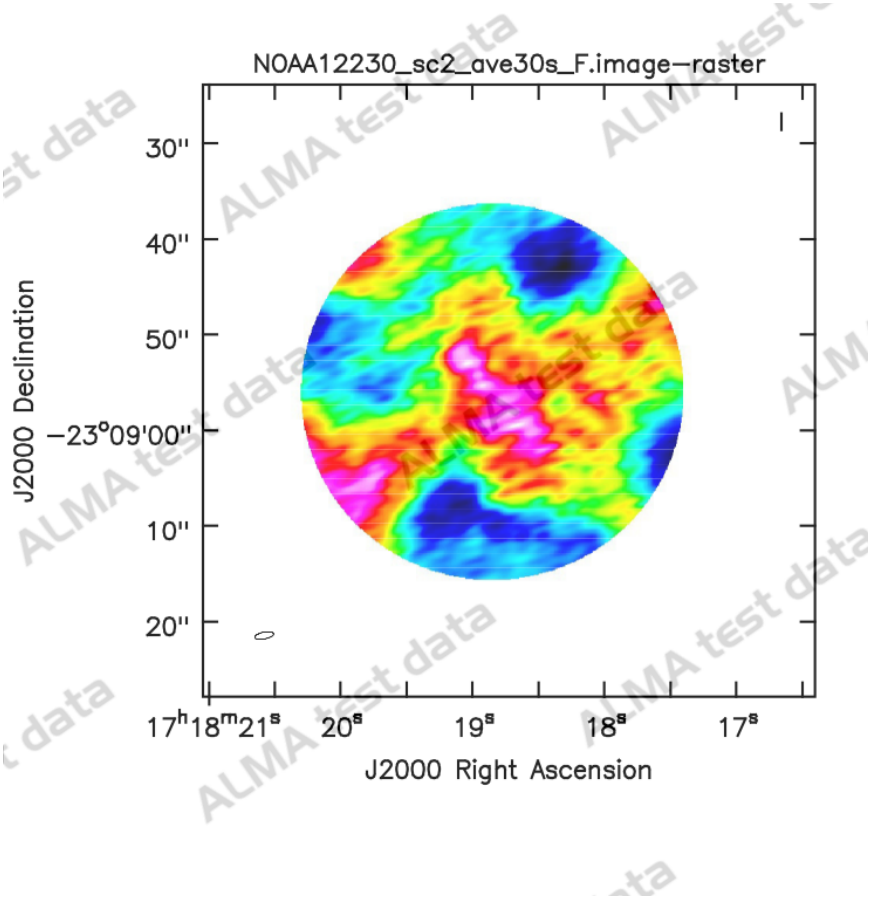

Figure 4.4 Image of NOAA12230 after CLEAN. Generated using CASA from solar observation uid://A002/X96b03d/X27f, which took part in December 12 2014 from 19:25 UT to 20:12 UT. The corresponding de-tuning mode is band6-solar2.

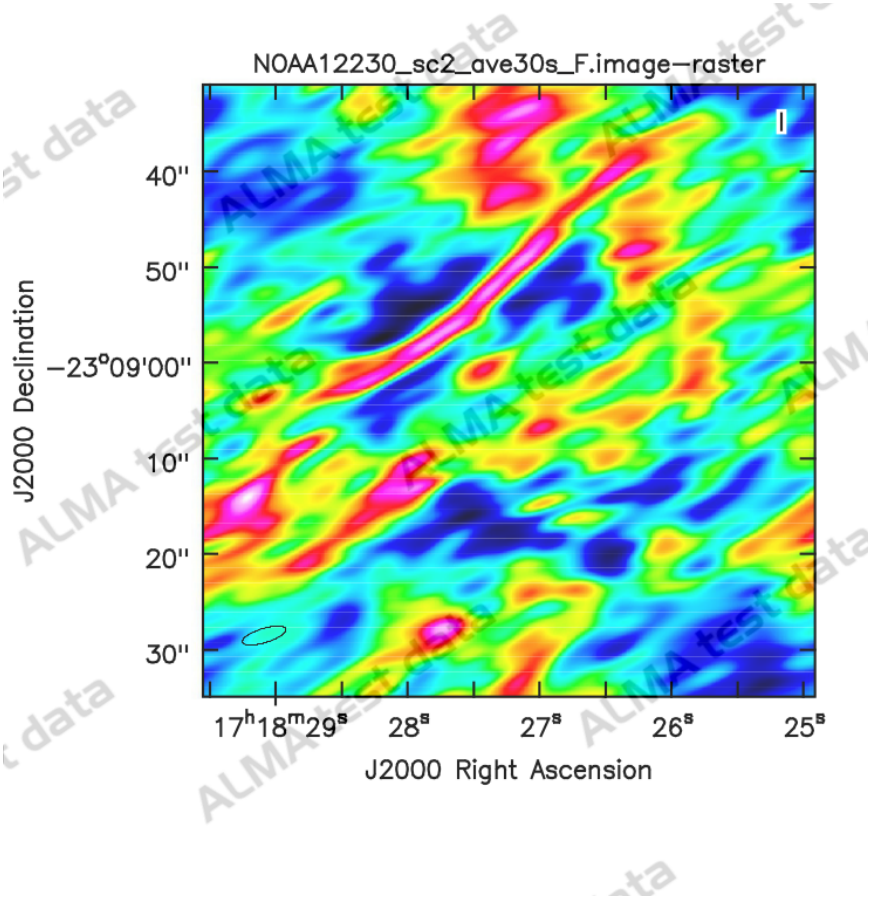

Figure 4.5 Image of NOAA12230 after CLEAN. Generated using CASA from solar observation uid://A002/X96b03d/X2d8, which took part in December 12 2014 from 20:12 UT to 21:00 UT. The corresponding de-tuning mode is band3-solar2.

An example of comparison between ALMA's results and other observatory's results is shown in Figure 4.6. These two images are provided by ASOC team member Timothy Bastian. A filament structure can be easily seen from both SDO's and ALMA's image, which gives a good sense of how well the ALMA's image can be related to other bands.

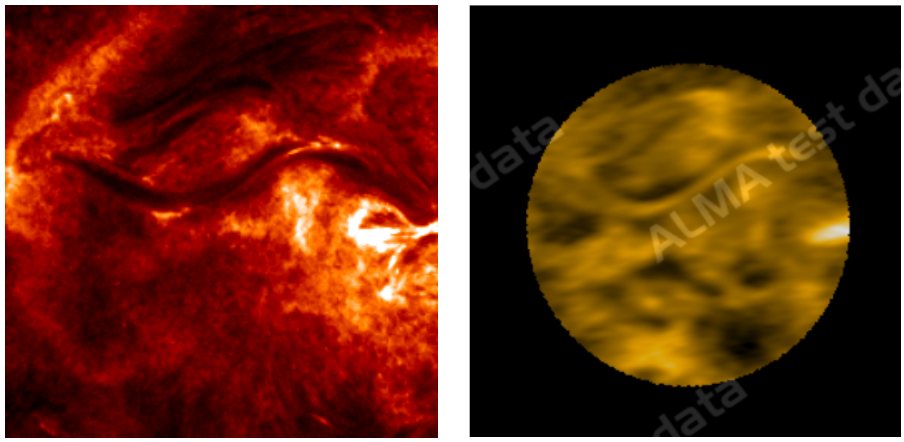

Figure 4.6 Images of the active region AR12230. The images are provided by ASOC team member Timothy Bastian. The right-side figure was taken on December 12 2014 with ALMA (band 3), and the left-side Figure is from SDO AIA304, with observing wavelength equals to 304 angstroms.

CHAPTER 5

DISCUSSION

In this thesis, the author has given an overview of the instrumental characteristics of ALMA, and the special considerations required to obtain scientifically useful data on the Sun. The author has also described results of the ALMA Solar Observing Campaign, which is an initial study designed to commissioning ALMA for solar observations. The coming ALMA Cycle 3 does not include solar observations due to the fact that, until the study team completes its work and demonstrates to ALMA oversight committee that its observing strategies work, proposals for solar observations will not be allowed. The next opportunity for solar proposals is Cycle 4, which starts in October 2016, so the decisions about what solar mode will be involved should be made about one year earlier (September 2015). The problems that need to be solved are listed here: 1. Develop procedures for single-dish mapping of the Sun, and demonstrate that the CASA software tools can properly analyze the data. 2. Develop procedures for calibration of interferometric data, which requires that both Sun and calibrators can be observed with the same configuration. As described in Chapter 2, the solar filter turns out to provide too much attenuation, so that the signal to noise ratio on calibrators is too low for accurate calibration with the solar filter installed. To get around this problem the study team has developed and tested several tuning modes (see Table 2.1), which provide optimal settings for most quiet Sun and flare observations. 3. Ensure that the required coordinate transformations are available in the pre-planning software (Observing Tool) and in the post-processing software (CASA) so that proposers can make effective use of the instrument.

The results described in this thesis demonstrate several successful strategies for solar observing. Fast scanning in either Lissajous or Double Circle patterns provide single-dish observations that can cover large parts of the Sun quickly enough to resolve

solar oscillations, and to detect flares for potential repointing of the other dishes to a flaring location. Currently, the data analysis of single-dish observation is done in third-party software such Matlab or IDL, and it is still under consideration whether some tools within CASA are needed. The SIS mixer de-tuning modes for calibrating interferometric data have been developed and shown to work (Figures 4.3 4.4 4.5 4.6), although no flaring emission has yet been imaged.

The coordinate system that ALMA uses for observation is sidereal coordinates (RA, Dec). However the Sun is moving with respect to the celestial coordinates, which causes difficulties in using CASA to generate correct coordinates. The study team is working on how to use CASA to produce images with coordinates in the Sun-centered, heliographic coordinate system familiar to solar researchers. A similar problem exists for planning observations, where a solar target in heliographic coordinates must be translated to the sidereal coordinate system understood by the ALMA control system. Thus, the study team must develop requirements documents that prescribe what capabilities the Observing Tool must have prior to the start of the Cycle 4 call for proposals.

The solar science goals that ALMA will address has also been introduced in the thesis. The initial images produced during the ALMA Solar Observing Campaign are promising, but a requirement of the ALMA study teams is that no science may be done with the test data, by members of the study team or anyone else. For that reason, images in this thesis are required to be water-marked, and can only be used in demonstrating instrument performance. Nevertheless, the glimpse of the potential for science with ALMA provided by these tests amply demonstrates the huge solar science impact ALMA will have.

APPENDIX A

MATLAB SCRIPT

Matlab script for generate interpolated image of single-dish data.

```
function [I]=imageshow(data,i)

%for default setting, data from column 4 is used
if nargin==1
    i=4;
end

%create a scatter map to show the scan pattern
scatter(data(:,2),data(:,3),5,data(:,i));
colorbar;

figure;
[x,y]=meshgrid(150:1:700,-600:1:-50);
I=griddata(data(:,2),data(:,3),data(:,i),x,y);
imshow(I,[]);

end
```

APPENDIX B

CASA SCRIPT

CASA script for calibration and imaging of interferometer data.

```
asdm ='name of the asdm file'

#Switch for each process
imp       = 'F'
calib     = 'F'
cal1_img  = 'F'
cal2_img  = 'F'
sun_img   = 'F'
#primary beam correction switch
pbc       = 'F'

#Setup parameters
flaggedantenna ='flaggedantennas'
mso = asdm + '.ms'
sp1 = asdm +'_split'
mso1 = sp1+'.ms'
ms1a = sp1+'_ave.ms'
ms1b = sp1+'_ave_scan2.ms'



#preparation of the data
if imp =='T':

    #import asdm to MS2
```

```
importasdm(asdm = asdm, vis = mso)

#correct the ephemeris
fixplanets(vis=mso,field='0',fixuvw=True,refant='DV10',
reftime='median')

#dump of the observing information
listobs(mso, listfile = asdm + '_listobs.txt')

#make the plot of the antenna configuration
plotants(mso, figfile= asdm + '_antconf.png')

#make a cal-table from Tsys data
gencal(vis = mso, caltable = asdm + '_tsys.tbl',
       caltype = 'tsys', spw='1,3,5,7')

#make the plots of Tsys
plotbandpass(caltable=asdm + '_tsys.tbl',
             overlay='antenna',plotrange=[0, 0, 40, 240],
             figfile='Tsys_zoom.png', interactive=False)
plotbandpass(caltable=asdm + '_tsys.tbl',
             overlay='antenna',plotrange=[0, 0, 40, 4000],
             figfile='Tsys_overall.png', interactive=False)
plotbandpass(caltable=asdm + '_tsys.tbl',overlay='antenna',
             antenna=flaggedantenna,plotrange=[0, 0, 40,
4000],
             figfile='Tsys_flaggedantenna.png', interactive=
False)
```

```
#Start Calibration
if calib =='T':

    #flagging caused by anomalous Tsys
    flagdata(vis = mso, mode='manual',
             antenna=flaggedantenna, flagbackup = T)

    #Apply the Tsys cal-table.
    applycal(vis = mso, interp='linear,spline',
             gaintable=asdm + '_tsys.tbl',spw='1,3,5,7')

    #########
    #Note: WVR correction is not executed, beause 7m-antennas don
    't have WVR system.
    #########

    #Extract only ch:50~200 data to avoid the influence of the
    edge chennels (TDM)
    split(vis=mso, outputvis=mso1, datacolumn='corrected',
          spw='1:50~200,3:50~200,5:50~200,7:50~200')

    #plot of the data for manual flagging.
    #plotms(mso1, antenna='*&*')

    #####
    #At first, stop the script at the point.
    #####

    #flagging the auto correlation data
```

```
 flagdata(vis = mso1, mode = 'manual', autocorr=T, flagbackup
= F)

 #flagging caused by the dispersion of the calibration results
 #flagdata(vis = mso1, mode = 'manual', scan='18~23',
flagbackup = F)

 #save flagging data
 flagmanager(vis = mso1, mode = 'save',
             versionname = 'Orginal', comment = 'Original')

 #Make gain cal-table (phase only) for making bandpass cal-
table
 gaincal(vis = mso1, caltable = sp1 + '_G0.tbl', spw='*:50~100
',field = '2',
         gaintype = 'G', calmode = 'p', refant = 'DV10',
solint='int')

 #plot Gain cal-table
 plotcal(caltable = sp1 + '_G0.tbl', yaxis='phase',
         iteration='antenna',  subplot=221)

 #make bandpass cal-table
 bandpass(vis = mso1, caltable = sp1 + '_B1.tbl', field = '2',
          refant = 'DV10', solint='inf',combine='scan',
          gaintable = [sp1 + '_G0.tbl'])

 #plot bandpass cal-table
 plotbandpass(caltable=sp1 + '_B1.tbl',
```

```
                overlay='antenna',plotrange=[0, 0, -90, 90],
                yaxis='phase',xaxis='freq',
                figfile=sp1+'_B1_phase.png', interactive=False)
    plotbandpass(caltable=sp1 + '_B1.tbl',
                overlay='antenna',xaxis='freq',yaxis='amp',
                figfile=sp1+'_B1_amp.png', interactive=False)

    #make Gain cal-table
    gaincal(vis = mso1, caltable = sp1 + '_G1.tbl', field = '2',
            gaintype = 'G', calmode = 'ap',
            gaintable = [sp1 + '_B1.tbl'],refant = 'DV10')

    #plot Gain cal-table
    plotcal(caltable =  sp1 + '_G1.tbl', xaxis='time', yaxis='amp
    ',
            iteration='antenna',subplot=221)
    plotcal(caltable =  sp1 + '_G1.tbl', xaxis='time', yaxis='
    phase',
            iteration='antenna',subplot=221)

    #apply cal-tables
    applycal(vis = mso1, gaintable = [sp1 + '_B1.tbl', sp1 + '_G1
    .tbl'])

    #Time averaging for reducing the computating time.
    split(vis=mso1,  outputvis=ms1a, datacolumn='corrected',
    timebin='30s')

#Making image
```

```
if cal1_img == 'T':
    #Image synthesis for 1700-261 (phase calibrator)
    clean(vis = ms1a,
          field='2',
          spw='0',
          imagename='1700-261_all',
          cell = '0.1 arcsec',
          imsize = 640,
          weighting = 'briggs',
          interactive = T,
          npercycle = 100,
          niter = 1000,
          imagermode='mosaic',
          minpb=0.2,
          pbcor=True)

if cal2_img == 'T':
    #Image synthesis for 1733-130 (flux calibrator)
    clean(vis = ms1a,
          field='1',
          scan='12',
          spw = '0',
          imagename='1733-130_sc12',
          cell = '0.1 arcsec',
          imsize = 640,
          weighting = 'briggs',
          interactive = T,
          npercycle = 100,
          niter = 1000,
```

```
            imagermode='mosaic',
            minpb=0.2,
            pbcor=True)

if sun_img == 'T' and pbc == 'T' :
    #Image synthesis for sun

    #Delete all values in the pointing table
    #tb.open(ms1a+'/POINTING', nomodify = False)
    #a = tb.rownumbers()
    #tb.removerows(a)
    #tb.close()

    #spliting the scan that used for generation of the image
    split(vis=ms1a,ouputvis=ms1b,datacolumn='corrected',scan='2')

    #fixing the pointing
    fixplanets(vis = ms1b,
               field = '0',
               fixuvw = Ture,
               refant = 'DV10',
               reftime ='median')

    #Clean
    clean(vis = ms1a,
          field='0',
          scan='2',
          imagename='NOAA12230_sc2_ave30s_T',
          cell = '0.1 arcsec',
```

```
            imsize = 640,
            interactive = T,
            weighting = 'briggs',
            npercycle = 100,
            niter = 6000,
            imagermode='mosaic',
            minpb=0.2,
            pbcor=True)

    #make FITS file of the solar image
    exportfits(imagename='NOAA12230_sc2_ave30s_T.image',fitsimage
   ='NOAA12230_sc2_ave30s_T.fits')


if sun_img == 'T' and pbc == 'F' :
    #Image synthesis for sun

    #Delete all values in the pointing table
    #tb.open(ms1a+'/POINTING', nomodify = False)
    #a = tb.rownumbers()
    #tb.removerows(a)
    #tb.close()

    #spliting the scan that used for generation of the image
    split(vis=ms1a,ouputvis=ms1b,datacolumn='corrected',scan='2')

    #fixing the pointing
    fixplanets(vis = ms1b,
               field = '0',
```

```
                fixuvw = Ture,
                refant = 'DV10',
                reftime ='median')

#Clean
clean(vis = ms1a,
          field='0',
          scan='2',
          imagename='NOAA12230_sc2_ave30s_F',
          cell = '0.1 arcsec',
          imsize = 640,
          interactive = T,
          weighting = 'briggs',
          npercycle = 100,
          niter = 6000,
          imagermode='mosaic',
          minpb=0.2,
          pbcor=False)

#make FITS file of the solar image
exportfits(imagename='NOAA12230_sc2_ave30s_F.image',fitsimage
='NOAA12230_sc2_ave30s_F.fits')
```

REFERENCES

[1] Http://www.almaobservatory.org/en/about-alma/origins-of-the-alma-project/timeline Accessed: 2015-04.

[2] A. Remijan, M. Adams, and R. Warmels, Eds., *ALMA Cycle 3 Technical Handbook*, 2015.

[3] T. Wilson, K. Rohlfs, and S. Hüttemeister, *Tools of Radio Astronomy*. Springer-Verlag Berlin Heidelberg, 2014.

[4] J. Pardo, J. Cernicharo, and E. Serabyn, "Atmospheric transmission at microwaves (atm): an improved model for millimeter/submillimeter applications," *Antennas and Propagation, IEEE Transactions on*, vol. 49, 10 2001.

[5] T. Bastian, "Advanced solar observing techniques," National Radio Astronomy Observatory, Tech. Rep., 2014 NA ALMA Development Study Plan.

[6] P. A. Yagoubov, "Solar observations with alma-how to minimize saturation in sis mixers," *Infrared, Millimeter, and Terahertz Waves (IRMMW-THz), 2013 38th International Conference on*.

[7] Http://jira.alma.cl/browse/CSV-3167 Accessed: 2015-04.

[8] M. Shimojo, "Flux calibration for single-dish solar observations with the solar filter," National Astronomical Observatory of Japan, Tech. Rep., 2014. [Online]. Available: https://jira.alma.cl/browse/CSV-2926

[9] Https://wikis.alma.cl/bin/view/CSV/FastSingleDishMappingObservatoryCalibration Accessed: 2015-04.

[10] S. Thornton and J. Marion, *Classical Dynamics of Particles and Systems*, 5th ed., 2004.

[11] Http://www.naic.edu/general Accessed: 2015-04.

[12] Http://fast.bao.ac.cn/en/ Accessed: 2015-04.

[13] Https://science.nrao.edu/facilities/vlba Accessed: 2015-04.

[14] A. Beasley, "Alma antenna naming and pad identification schemes," Tech. Rep. [Online]. Available: https://safe.nrao.edu/wiki/bin/view/ALMA/CalAncillary

[15] Http://jira.alma.cl/browse/CSV-3166 Accessed: 2015-04.

[16] J. Ott, Ed., *CASA User Reference and Cookbook*, 2014.

[17] A. R. Thompson, J. M. Moran, and G. W. Swenson Jr, *Interferometry and synthesis in radio astronomy*, 2nd ed. Wiley, 2001.

[18] R. N. Bracewell and J. A. Roberts, "Aerial smoothing in radio astronomy," *Australian Journal of Physics*, vol. 7, no. 4, pp. 615–640, 01 1954.

[19] J. A. Högbom, "Aperture synthesis with a non-regular distribution of interferometer baselines," *Astronomy and Astrophysics Supplement Series*, vol. 15, p. 417, 1974.